IRAM Working Report No. 228/95

Frequency Switching at the 30m Telescope

C. Thum, A. Sievers, S. Navarro, W. Brunswig, J. Peñalver

13–May–1995

Abstract

During several test periods in 1994 we investigated the hardware and software involved in frequency switching observations at the 30m telescope. All four standard spectroscopy receivers were made to frequency–switch correctly, but only two of them, the 3mm and/or the 1mm receiver No.1, can currently be used in actual frequency–switching observations. The spectroscopic baselines are good at 3mm, but were found sufficiently flat in all cases investigated, provided some precautions are taken as described in this report.

The technical limitations for the principal frequency switching parameters, the throw and the switching rate, were identified. The maximum throws range from about 45 $\mathrm{km\,s^{-1}}$ at 3mm to near 70 $\mathrm{km\,s^{-1}}$at 1mm. Switching rates are limited by the correlator acquisition to a maximum of 1.0 Hz. The time efficiency of frequency switching observations exceeds 90%.

We have observed the 1mm emission line of mesospheric CO as an external frequency standard. The overall precision of the observatory's frequency tracking is better than 15 kHz.

Contents

Chapter 1

Introduction

The frequency switching technique is of great potential interest to the millimeter spectroscopist, since it combines important advantages over other observing modes. It is very efficient, since 100% of the observing time is spent on source, it can be used for very extended sources (no emission–free reference field needed), it provides better cancellation of atmospherice emission fluctuations due to potentially higher switching speeds, and it makes sideband identification a trivial matter.

Despite these assets frequency switching (FSw) was not used much at the 30m telescope in the past, primarily because FSw spectra tended to have poor spectroscopic baselines. This problem is probably due to an increased sensitivity of FSw observations to power instabilities of the receivers. Other problems can arise if the line of interest is wide (or if it is embedded in an emission feature which is broad) compared to the frequency throw available, or if it is confused with atmospheric emission. In section 6.2 we give a short guide as to when FSw observations are practical.

During 1994, motivated in part by the arrival of a new generation of SIS receivers, we have made several test runs with the aim to bring the FSw equipment and its control software up to date, to find out what the limits are for the various FSw parameters, and last, but not least, investigate the quality of the spectroscopic baseline for FSw observations. Nine intervals of about 8 hours of daytime each were allocated to this effort in 1994. During 12 hours of this technical time the telescope could be used on the sky. During the rest of the time, other technical work blocked the telescope in zenith (3 intervals), or bad weather (3 intervals) or other work (1.5 intervals) prevented observations altogether.

The tests concentrated on the simplest mode of frequency switching where two equally long phases have the same amount of frequency offset from the nominal sky frequency, but opposite directions ("symmetrical FSw"). More complicated switching schemes are conceivable, but have not been tested. Although all standard spectroscopy receivers on the 30m telescope have been made to frequency switch corrrectly, only two of them, the 3mm SIS and the 1.3mm SIS No. 1 (i.e. those served by the main polarization grid in *transmission*, see Fig. 2.1), could be investigated in any detail within the available time.

In this report we first describe the technical background relevant for frequency switching (section 2) and then show that reasonable spectroscopic baselines can now be obtained if some precautions are taken (section 3). In section 4 we investigate the various instrumental limitations specific to the present FSw hardware, and section 5 discusses mesospheric emission. The appendix lists useful observing and data reduction procedures.

Chapter 2

Technical Implementation

Here we describe the various hardware components which are relevant for frequency switching observations. The description refers to the situation in December 1994 when the tests were concluded.

2.1 Receivers and Local Oscillators

This report is concerned only with the four standard spectroscopy receivers: *(i)* the 3mm receiver (henceforth referred to as the `3MM`), *(ii)* the two 1.3 mm receivers (`G1` and `G2`), and *(iii)* the 2mm receiver (`2MM`). The arrangement of these receivers in the Nasmyth cabin of the 30m telescope is shown in Fig. 2.1. The Nasmyth optics is presently set up in such a way, that the receivers `3MM` and `G1`, i.e. those which are served by the main polarization grid in transmission, observe in parallel owing to a diplexing element in combination with a polarization grid. The movable mirror M5 selects one of the two receivers, `2MM` or `G2`, served by the main grid in reflection. This setup allows the simultaneous operation of up to three receivers.

All receivers have a very similar local oscillator scheme (Fig. 2.2). A CAMAC driven low noise ADRET synthesizer[1] generates a signal near 100 MHz whose frequency is controlled with a resolution of 10 Hz ($\sim 1 \cdot 10^{-7}$). In the reference No. 1 branch, this signal is then multiplied in the lock source by a constant factor (48) in order to pump the subsequent harmonic mixer. The n^{th} harmonic of this signal ($n \sim 17$) is then in the 3mm band of the Gunn oscillator. A sample of its output is combined in the harmonic mixer with the ref. 1 signal to generate a frequency and phase difference signal. The difference signal is then compared in a XL Microwave Phase Lock module with a second reference frequency, generated in an identical ADRET synthesizer. The Gunn oscillator output constitutes the local oscillator signal, either directly as in the case of the 3mm receiver or after passage through a frequency multiplier (factor m) as in the case of the other receivers. The LO frequencies are thus quantised in steps of $\sim m \times 8.2$ kHz.

2.2 Frequency Switching Hardware

At the 30m telescope, frequency switching is effected by moving the frequency of the reference No. 2 ADRET synthesizer (same model as in ref. 1 branch) under control of the

[1] The observatory plans to replace the ref. 1 synthesizers in the near future by higher performanance models.

FSw module (Fig. 2.2). The ADRET output frequency is normally set to a value near 100 MHz in non–FSw observations, i.e. at the center of the module's tuning range from 90 (80 in some newer models) to 120 MHz. This range gives directly the limit to the maximum throw in sky frequency for the receivers without a multiplier (like the 3MM). If a muliplier (factor m) is used, the maximum throw is $m \times 30(40)$ MHz on the sky. Similarly, the ref. 2 module's frequency resolution (nominally 10 Hz, but only controlled down to the 100 Hz digit) gives directly the resolution in sky frequency ($m \times 100$ Hz). The frequency quantization due to the ref. 2 synthesizer is thus much smaller than the quantization due to the ref. 1 module. The ref. 1 synthesizer is therefore used for fine–correction of the LO frequency.

The FSw module is a custom designed dual–slot CAMAC module whose task is to provide the necessary interface, for up to two independent ADRET synthesizers, between the acquisition program and the receiver hardware. It can handle up to four different frequencies (for 4–phase FSw), and it produces the timing signals for each phase and a blanking line that will remain active during the phase transitions. One additional such FSw module working in a master–slave configuration is available for controlling up to four receivers independently. The time it takes to move the ADRET output from one frequency to another depends in a complicated on the exact value of these frequencies and their difference, but it is smaller than 10 msec in most cases of interest for FSw observations. The blanking time was therefore fixed to this value.

Frequency switching could, in principle, also be done with the ADRET synthesizer in the ref. 1 branch. This solution would however have the disadvantages of *(i)* introducing the $m \times 8.2$ kHz frequency quantization in the frequency throw, and *(ii)* making the switching somewhat slower since one additional component (the lock source) has to move.

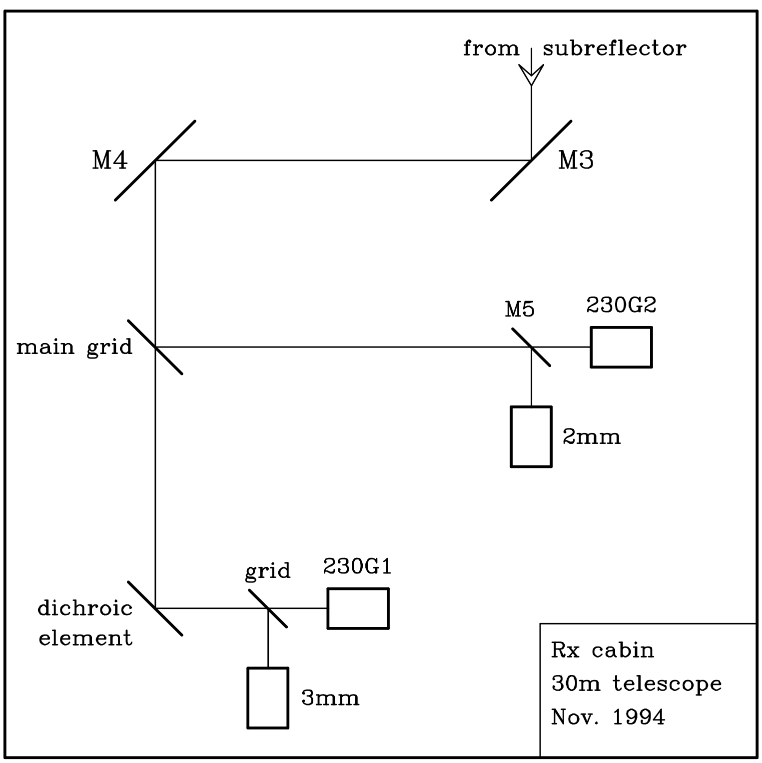

Figure 2.1: Schematic diagram of the receiver cabin of the 30m telescope. Only the standard SIS receivers are shown. The main grid transmits horizontal, and reflects vertical linear polarization. The combination of a diplexing element and a grid (a "dichroic" element) allows the 3MM and G1 receivers to observe simultaneously. The movable mirror M5 selects the 2MM or the G2 receiver.

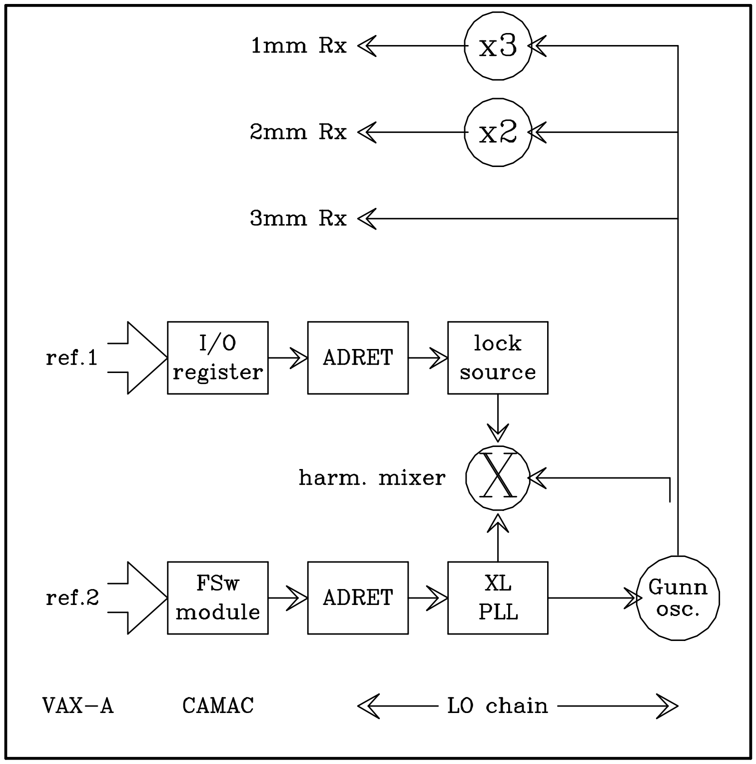

Figure 2.2: Layout of the local oscillator chain. The ADRET generates a signal near 100 MHz. The lock source in the ref. 1 branch multiplies the input by a factor 48. The ADRET in the ref. 2 branch is frequency switched under the control of the FSw module built by J. Peñalver. The phase lock PLL (model XL) controls the Gunn oscillators whose output is multiplied before coupling into the shorter than 3mm wavelength receivers.

2.3 Receiver Stability

Some measurements of the stability of the receivers were carried out with the idea that the less stable receivers may also show a larger power imbalance in frequency switching, and may thus have poorer spectroscopic baselines. Table 2.1 summarizes the results for the four standard receivers and for the most popular line frequencies. The receivers were SSB tuned in the usual way with the recommended USB rejection factors. The peak–to–peak IF power fluctuations ΔT_{Rx} were measured on the chart recorder for time scales of 1 sec and 1 min, and calibrated with the usual ambient and liquid nitrogen temperature loads. For measurement of the imbalance, frequency switching was started with phase durations of 1.5 sec and throws as noted in the table. The difference of IF power in the 2 FSw phases, the imbalance, was again measured from the chart recorder and calibrated as before.

The stability measurements are summarized in Fig. 2.3a. We find that the 3mm receiver has clearly the best stability with values of Δgain $\leq 10^{-3}$ on the 1 sec time scale, followed by the receiver `G2`. The `3MM` receiver has also, by a large margin, the best baseline performance (see section 3). The `2MM` receiver shows the worst performance, particularly at the low frequency end of its tuning range. It may be significant in this context that this receiver is the only one at the observatory whose junction circuitry has not yet been converted from current–biased to voltage–biased.

Fig. 2.3a furthermore shows that the stability tends to decrease with decreasing frequency for all the standard spectroscopy receivers, and most strikingly, that the gain fluctuations are usually a factor ~ 3 larger at the 1 min time scale than at 1 sec, for all receivers and frequencies investigated. These correlations may be explained by one cause common to all receivers, that is LO power fluctuations. In a SIS receiver, these tend to generate in turn fluctuations of the IF power[2] which, for a given spectrum of LO fluctuations, are larger at

[2]Note that at the time of the tests none of the standard SIS receivers was equipped with any sort of gain control.

Table 2.1: Receiver gain fluctuations and imbalance. Receivers (noise temperature T_{Rx} are tuned to LSB (USB rejection factor g). ΔT_{Rx} are the peak–peak gain fluctuations. Measurements were made on 28/29 September 1994.

Rx	frequency GHz	line	T_{Rx} K	g dB	ΔT_{Rx}[K] 1 sec.	1 min.	imbalance K	throw MHz
	115.3	$^{12}CO(1\rightarrow0)$	106	25	0.12	0.24	1.47	7.88/2
3mm	110.2	$^{13}CO(1\rightarrow0)$	90	25	0.12	0.24	0.73	7.88/2
	86.2	SiO(v1; J:2-1)	130	30	0.30	0.70	6.26	7.88/2
	220.4	$^{13}CO(2\rightarrow1)$	130	10	0.54	1.08	40.5	7.88*1.5
G1	230.6	$^{12}CO(2\rightarrow1)$	183	10	0.18	1.44	16.9	7.88*1.5
	244.9	CS(J: 5-4)	230	10	0.61	1.91	7.69	7.88*1.5
	131.0	—	90	7	2.57	9.00	20.6	7.88
2mm	147.0	CS(J: 5-4)	145	7	0.50	1.24	8.94	20
							6.46	7.88
	220.4	$^{13}CO(2\rightarrow1)$	110	20	0.99	3.70	30.9	7.88*2
							14.8	7.88
G2	230.6	$^{12}CO(2\rightarrow1)$	80	20	0.24	0.88	2.25	7.88
							3.77	7.88*2
	244.9	CS(J: 5-4)	250	20	0.12	0.33	0.83	7.88
							4.87	7.88*2

lower frequencies, since the tuning peaks tend to be narrower there. We cannot exclude at this point, however, that 1/f–noise in the bias circuitry or in the post–detection chain also contributes to the observed gain fluctuations.

Fig. 2.3b demonstrates that there is little detailed correlation between gain stability and imbalance, although again the `3MM` and `G2` receivers perform best. In all cases the imbalance was at least a factor of 5 larger than Δgain(1sec), up to factors $\sim$ 100 in the worst cases (`G1`). As expected, the imbalance was always larger for the larger throws. The lack of a detailed correlation is a bit of a puzzle, but is tentatively attributed to strong fine structure of the bandpass.

Apart from the fact that the most stable receiver, the `3MM` receiver, has also a low imbalance and has clearly the best spectroscopic baselines (see section 3), the general relation between baseline ripple and imbalance could not be investigated in any detail due to lack of time.

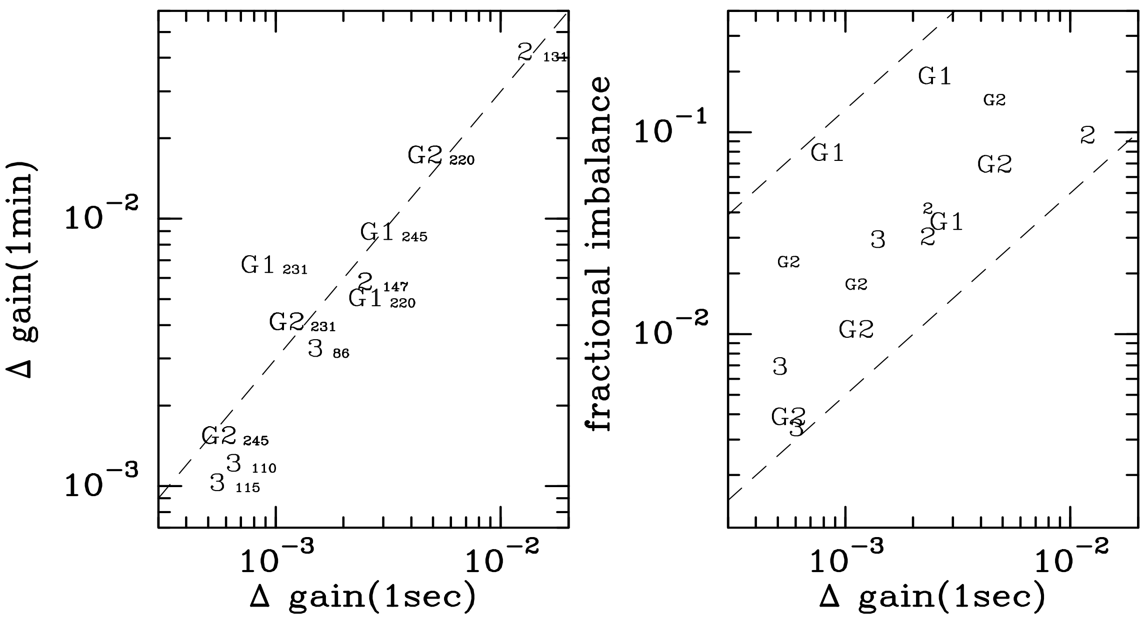

Figure 2.3: Stability of receivers. **(a)** relative (peak–to–peak) fluctuations on time scales of 1 sec and 1 min for the standard SIS receivers (3: `3MM`, 2: `2MM`, and `G1` and `G2` for the 1.3 mm receivers). The small numbers indicate the frequencies (in GHz) at which the measurement was made. The dashed line has a slope of 3. **(b)** Fractional power imbalance between the two phases in frequency switching for the standard receivers. Smaller symbols refer to the larger throws (Tab. 2.1). The two dashed lines have slopes of 5 and 100.

Chapter 3

Spectroscopic baseline

Frequency–switched observations have to deal with the same baseline problems as other spectroscopic observing modes, but in FSw these problems appear to be more critical. At the 30m telescope, best spectroscopic baselines are obtained with "Wobbler–switching" where a combination of slow telescope and fast subreflector motions is used to efficiently cancel any ripple down to a few milli Kelvin. Conceptually, the fast motions (typically 0.5 Hz) serve to suppress the variable ripple component which can originate in variations of the receiver gain and of the atmospheric emission. The slow motions serve to suppress the steady ripple which is caused by reflections inside the telescope structure, and is therefore not suppressed by wobbling the subreflector.

This neat ripple suppression scheme does not directly transfer to FSw observations. Firstly, FSw moves the spectrometer window across the receiver bandpass which is likely to have some fine structure. The difference between the two phases of such a FSw observation may therefore not be very flat. Second, the task of keeping the gain of a millimeter–wave receiver constant is normally difficult enough, even if all essential components are held "constant". In the case of FSw where the local oscillator frequency is periodically varied, the receiver stability can only get worse (section 2.3). Thirdly and most importantly, the steady ripple component is not normally suppressed. Nevertheless, as we show in this chapter, reasonably flat spectroscopic baselines can now be obtained even in FSw observations, provided some precautions are taken as we described in this chapter. Best baselines are obtained at 3mm, currectly the receiver with the highest stability.

3.1 The standard ripple

Experience with earlier observations has shown that the spectroscopic baseline ripple at the 30m telescope is usually dominated by a component of frequency near 7.8 MHz which originates in reflections between the receiver and the subreflector. Fig. 3.1 shows that this component is also present and dominant in the baselines of frequency–switched observations. Actually, the figure shows the difference between the two phases of the FSw observation in which the frequency throw Δf was set to 3.9 MHz, i.e. about half the frequency of the standard ripple. We measure a relative ripple amplitude (ratio of peak–to–peak ripple over system temperature) of

$$\frac{\Delta T_{pp}}{T_{sys}} = 1.2 \cdot 10^{-3}$$

Inasmuch as the ripple can be approximated by a pure sine wave, the true relative ripple amplitude is then about half this value.

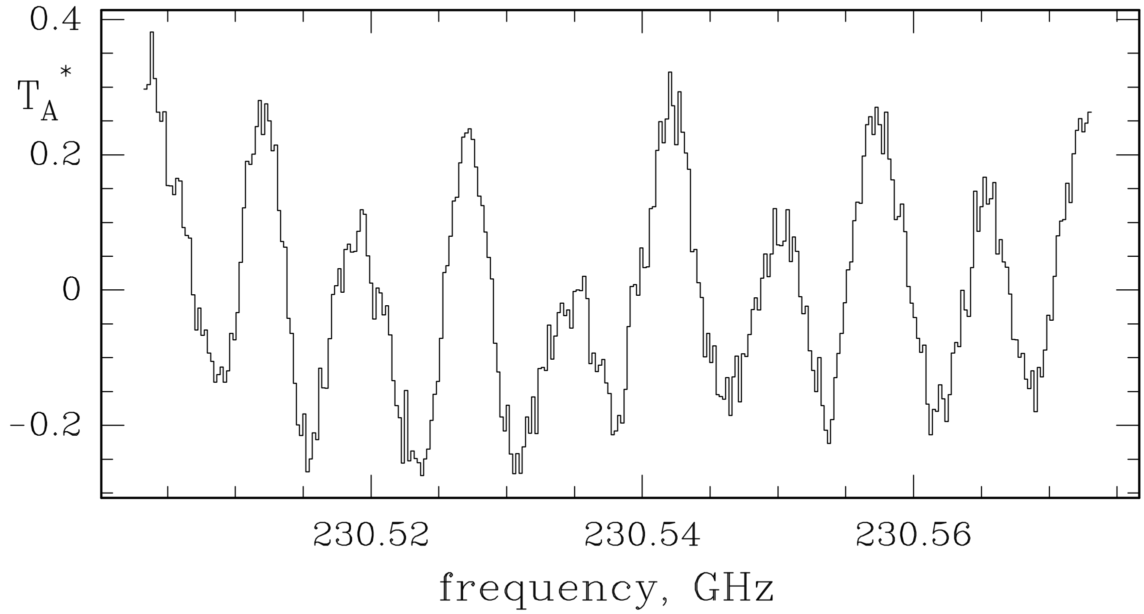

Figure 3.1: Typical example of spectroscopic baseline ripple observed on 21 July 1994 in the FSw mode with the 1mm SIS receiver No. 1, SSB (10 dB) tuned to $^{12}CO(2\rightarrow1)$. A FSw throw Δf of 3.9 MHz, i.e. about half the ripple frequency, was used to enhance the ripple amplitude. Integration time is 50 min. The autocorrelator backend was used with an effective bandwidth of 70 MHz and resolution of 234 kHz. During the observation the telescope was parked with all drives off, looking at zenith. The scattering cone was in place at the center of the subreflector, and an absorber ring was mounted around the outer 20 cm of the subreflector support box.

The ripple parameters were derived from a Fourier–transform of this spectrum. The three most clearly identifiable FFT components are listed in Tab. 3.1. The strongest component (path 19.6m) is the standard ripple between the receiver and the subreflector whose separation ranges from 19.10 m (subreflector vertex), to 19.46 m (subreflector edge), up to 19.71 m (subreflector support box). The accuracy of our measurement, half a FFT pixel or $\pm$0.2m, does not identify the scattering surface precisely, but suggests that most of the scattering occurs near the subreflector support box.

Component No. 2 is resolved at the resolution of our FFT, and its width is 0.8m centered at 9.7m. We think that several scattering paths (listed in Tab. 3.1) contribute to this component, the path between receiver and telescope vertex being the strongest.

Ripple Components No. 2 and 3 are factors 3 and 6 weaker than No. 1. This fact can be exploited to reduce the power contained in baseline ripples by a corresponding amount. The trick consists in making the frequency throw Δf equal to the frequency of the dominant ripple, i.e. 7.65 MHz, or a small integer multiple of it. Most of the test observations were actually made with such throws. The amplitude of the baseline ripple was found to be reduced at least a factor 3 in all cases.

In a special experiment, the ripple amplitude was measured as a function of Δf. When Δf was varied between $1\times\Delta f$ and $2\times\Delta f$, the amplitude was found to describe a sine wave with its maximum at $1.5\times\Delta f$, and approaching a small value again at $2\times\Delta f$. This behavior demonstrates again that the baseline ripple is indeed dominated by one frequency.

The fact that the ripple is still substantially reduced when using even $2\times\Delta f$ can be exploited when observing with the `3MM` and the `G1` receivers simultaneously, like for observations of CO transitions. An identical *velocity* scale is obtained in the two spectra if the `3MM` receiver is switched with $1\times\Delta f$ and the `G1` receiver with $2\times\Delta f$ while still maintaining

Table 3.1: Parameters of ripple components. The reflecting surfaces refer to the receiver (Rx), the subreflector area (sub), and the telescope vertex (V).

component No.	frequency [MHz]	path [m]	relative amplitude	reflecting surfaces	separation [m]
1	7.65	19.7 ± 0.2	1.00	Rx — sub	19.10...19.71
2	15.5	9.6 ± 0.4	0.30	Rx — V	9.29
				V — sub	9.8...10.4
3	4.85	31.0 ± 0.3	0.15	Rx—sub—V	~ 30

a substantial degree of ripple suppression. See appendix A for details and Fig. 6.1 for an example.

3.2 Xoptics

A frequently used procedure for reducing the intensity of a reflected wave employs the fact that reflection changes the sense of a circularly polarized wave. In the 30m telescope where all standard spectroscopy receivers have linearly polarized feed horns, this procedure can also be used under certain circumstances. They imply a slightly non–standard setting of the Nasmyth optics, here referred to as *Xoptics*. In contrast to the standard Nasmyth optics (*Soptics* for short) where the incoming wave is split between the `3MM` and `G1` receivers with the help of a polarization grid and a dichroic polarization rotator (Fig. 2.1), *Xoptics* removes the main polarization grid and sets the dichroic element to a non–standard grid/mirror separation, $\Delta = \lambda/4$. Tab. 3.2 summarises the two optics settings. In Xoptics, the dichroic acts as a quarter–wave plate, i.e. circular polarisation is converted into linear polarization.

Table 3.2: Two settings of the Nasmyth optics

	grid	dichroic element
Soptics	IN	$\lambda/2$
Xoptics	OUT	$\lambda/4$

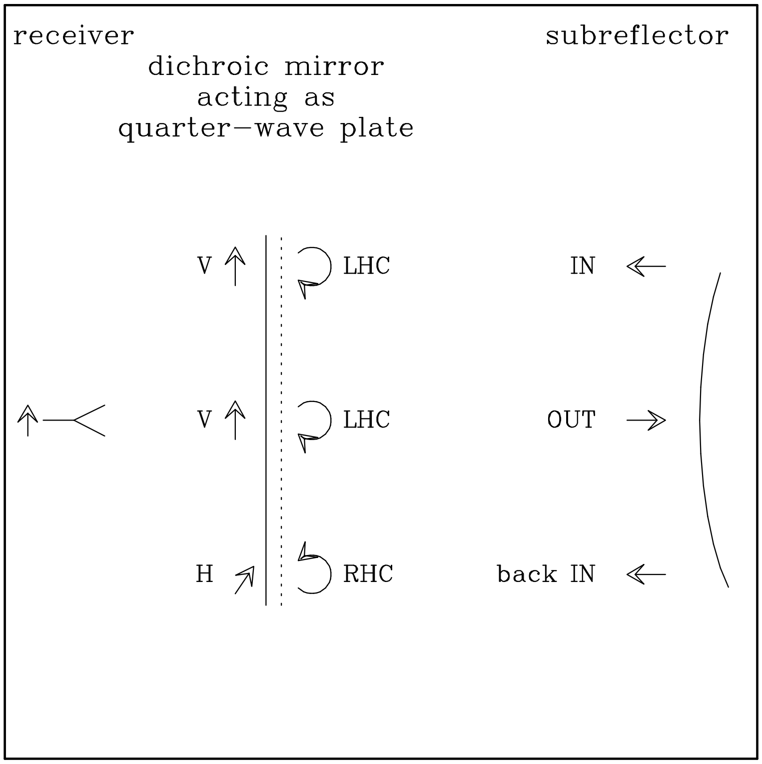

Figure 3.2: Special Nasmyth optics setup (Xoptics). The dichroic element which normally acts as a polarization rotator now acts as a quarter–wave plate. Furthermore in Xoptics, the main polarization grid is removed. Xoptics helps to suppress the wave reflected from the subreflector which would normally contribute to the baseline ripple. See text.

Fig. 3.2 shows schematically how Xoptics works in the 30m telescope. The dichroic element converts a LHC incoming wave (`IN`) into vertically (`V`) linearly polarisation which can be absorbed by the feed horn. The fraction of the incoming wave which is reflected from the feed horn (or any power *emitted* by the receiver) is converted back into LHC at the dichroic, changes into RHC upon reflection off the subreflector, and is then converted to H–linear by the dichroic. Since H–linear polarisation is not absorbed by the V–type feed horn, the reflected power which would otherwise contribute to the baseline ripple is rejected.

Several experiments were made to test the efficiency of this Xoptics scheme. The example shown in Fig. 3.3 demonstrates that at 1mm a substantial (factor 10) suppression of the ripple is achieved whereas at 3mm the suppression is no more than a factor 2. In all experiments, acceptable baselines were obtained, including at 1mm. Note however that virtually no integrations longer than 10 min were made on a celestial source due to lack of test time. A small baseline modulation ($\sim$ 8.5 MHz) is apparent at 3mm. It is not suppressed neither by Xoptics nor by the use of the optimum Δf, but its origin was not further investigated. A baseline offset and a linear slope have also survived all our ripple suppression schemes at 1 mm. These problems are however not very critical for obervations of narrow lines.

3.3 Dual receiver mode

The Xoptics scheme makes use of the dichroic element set to $\Delta = \lambda/4$. This demands the selection of one particular wavelength and thus normally precludes simultaneous observations at different wavelengths. Furthermore, since Xoptics implies the removal of the main polarization grid, the receivers served by this element in *reflection* cannot be used

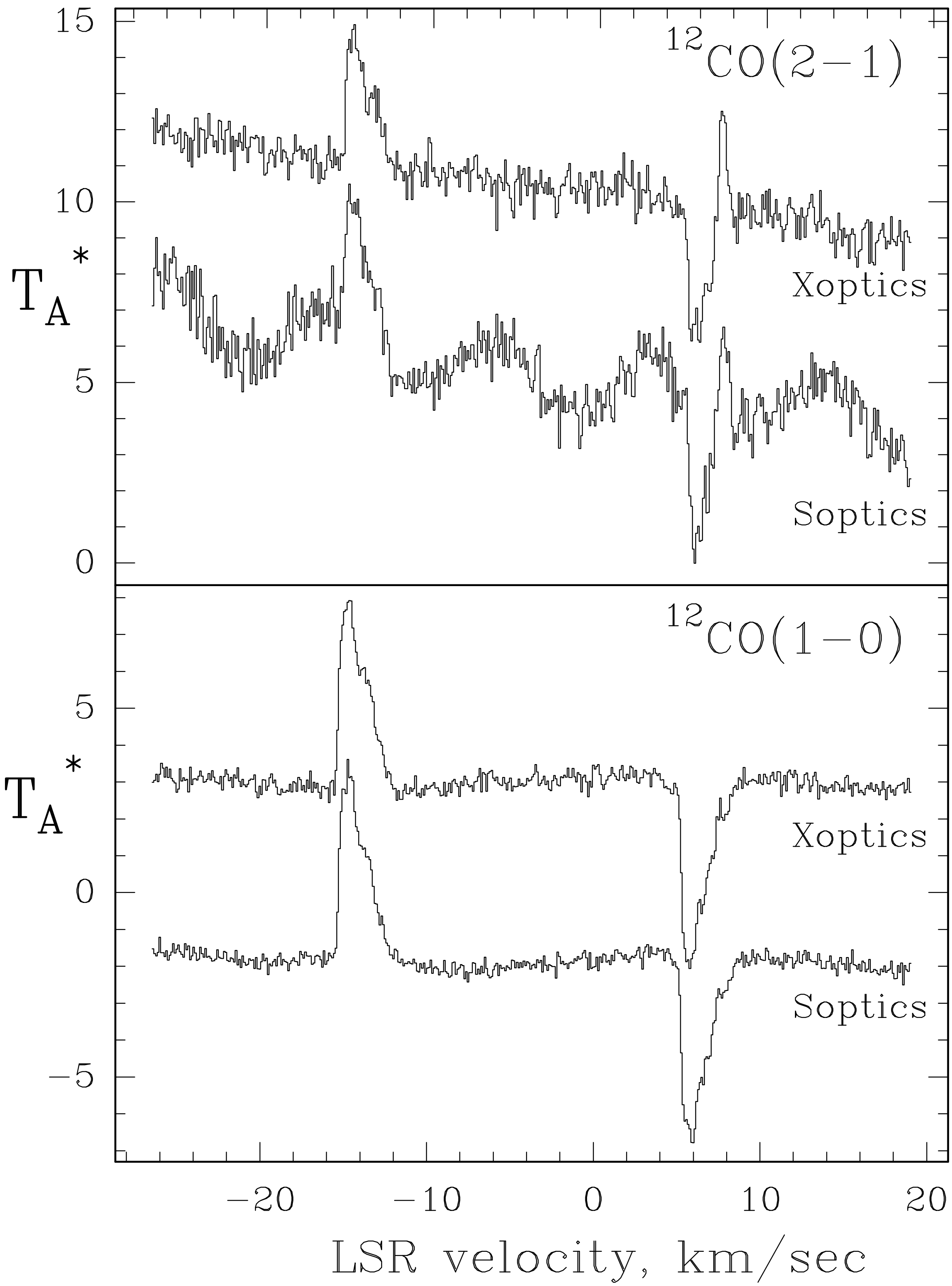

Figure 3.3: Dual receiver observation of the Polaris dark cloud. using Xoptics (see section 3.2). Note the presence of mesospheric CO in the 1mm spectrum near 7.5 km s^{-1}.

either. Thus the Xoptics advantage seems to restrict observations to the use of *either* the 3mm receiver *or* the 1mm G1 receiver, both served by the main grid in *transmission*.

These severe restrictions can be relaxed considerably if the dichroic is set to $\lambda/4$ for the 1mm receiver. For the 3mm receiver the dichroic is then operating near $\lambda/8$. The linear polarization of the 3mm feed horn is thus transformed into elliptical polarization. The circularly polarized component of this generally elliptically polarized wave behaves as before, and the baseline ripple is reduced correspondingly. The suppression of the 3mm ripple is therefore not as efficient as if the dichroic was tuned to the 3mm wavelength (as if only this receiver was used). But the resulting baseline is usually still quite acceptable, because 3mm baselines are intrinsically better than at 1mm probably due to superior stability of the present 3mm receiver.

Chapter 4

Instrumental limitations

A frequency switched observation is characterized primarly by the frequency throw and by the switching rate. Here we investigate the range in which each parameter can be varied, and we identify the component which currently limits this range. In the last section, we measure the efficiency of frequency switched observations under typical observing conditions.

4.1 Frequency Throw

The switching of the observing frequency is effected by switching the the ADRET (type 5104) synthesizer of the reference No. 2 branch between two fixed values (see section 2). The tuning range of this type of synthesizers starts at 90.000 MHz (old model) or 80.000 MHz (new model), and terminates at 119.999 MHz. In the present setup, not all of this range is exploited. In phase 1 of a (2 phase, symmetrical) FSw cycle, the synthesizer is set to about 100.0 MHz (see section 2.2) and in phase 2, it is normally set to a higher value, $100 + \Delta f$. thus limiting the maximum throw to a value near 19.9 MHz.

With one exception, all of the following components of the LO chain (Fig. 2.2), notably the phase lock, Gunn oscillator, an eventual multiplier, and the mixer can handle this throw. In the case where no further multiplication is involved (i.e. the 3mm receiver), this value is therefore also the current maximum frequency throw at the level of the sky

Table 4.1: Maximum frequency throws for `3MM` and `G1` receivers.

required typically		7.7, 15.4	MHz	(see Tab. 3.1)
synthesizer	now	$-10 \ldots +20$	MHz	old model
		$-20 \ldots +20$	MHz	new model
PLL	3mm	$-10 \ldots +17$	MHz	
	G1	$-20 \ldots +20$	MHz	
receiver	3mm	$-26 \ldots +45$	$\mathrm{km\,s^{-1}}$	at 115 GHz
	G1	$-70 \ldots +70$	$\mathrm{km\,s^{-1}}$	at 230 GHz

Table 4.2: Signal loss at high switching rates.

source	throw MHz	phase duration msec	signal loss [%]	signal loss msec
mesospheric $^{12}CO(2\rightarrow1)$	7.9	100	6 ± 1	6
artificial line at 115 GHz	7.9	50	12 ± 1	6
mesospheric $^{12}CO(2\rightarrow1)$	3.8	50	5 ± 1	2.5

frequency. For receivers which employ multipliers, the maximum throw in sky frequency is then twice (`2MM` Rx) or thrice (`G1` and `G2` Rxs) this value.

In the case of the `3MM` receiver, however, we found that the phase lock cannot handle throws larger than +17 MHz. In a very approximate manner, the maximum presently usable throw is +45 km s^{-1}, independent of observing frequency. A more accurate summary is given in Tab. 4.1 which is also used for the limits implemented in the OBS FSw command.

4.2 Switching Rates

The rate at which the reference No. 2 synthesizer is switched between the two frequencies in a cycle is controlled by the FSw CAMAC module (Fig. 2.2). An internal switch in this module selects one of three possible basic phase durations: 1, 10, and 100 msec. The module derives its time from a LC–type oscillator. The actual phase duration is then the basic phase duration multiplied by an integer number in the range 1...256 sent by the antenna control computer. This set up therefore permits phase durations in the range from 1 msec to 25.6 sec. In practice, since the internal switch is usually set to 10 msec, phase durations in the range from 0.01 to 2.56 sec can be used.

We investigated how much of this theoretically available range can actually be used. Inspection of the data sheet of the ADRET synthesizer, the first critical component in the LO chain (Fig. 2.2), shows that it takes typically 9 msec to move to a new frequency. During this time, no useful data can be obtained, and consequently the blanking signal provided by the module was set to a fixed 10 msec. The minimum useful phase time is then of the same order.

In the case where the synthesizer settling times are actually longer than advertized in the data sheet, the acquisition program would collect data during times when the LO is not at its expected values. The same problem would occur if any of the components following the reference No. 2 synthesizer would have a time constant larger than 10 msec for tracking frequency changes of the size typically encountered in frequency switching. We have tried to measure the resulting loss of signal in three experiments (Tab. 4.2). Each consisted in a series of observations with identical set up (frequency throw, 100 kHz backend) covering the full available range of phase times. The result is given as the percentage drop of signal at the shortest phase time used in the respective experiment relative to the signal at long phase times. This drop corresponds to a certain time interval, given in the last column of Tab. 4.2, during which the LO is not at its destination frequency. These data show that the measured losses are small, of the order of 10% at the shortest meaningful phase times. They are even negligible ($\lesssim$ 2%) at more typical phase times around 1 sec.

The measurements in Tab. 4.2 indicate, however, that there may be a component with a settling time of 2 . . . 6 msec longer than our blanking time of 10 msec. Its settling time may also depend on the size of the frequency throw. A few experiments were made to measure the time constant of the detector circuitry of the 100 kHz filter bank. They consisted in feeding into this filterbank a pulsed broadband noise source ("Gilles pulsar") which can be switched on and off with $< 1\mu$sec flanks at rates of 100 Hz under control of the station clock. A few channels of the filterbank were then recorded with the fastest sampling time available at the time, i.e. 6 msec. The flanks were not resolved, and we conclude that the 100 kHz detector circuitry is significantly faster than 6 msec.

Although the source of the signal loss is not positively identified, we believe that it originates in the longer settling times of the lower significant digits of the ADRET synthesizer. The 10 kHz and smaller digits which corresponded in our experiments to ~ 0.04 km s^{-1} or about 10% of the width of the signal line, have settling times of at least 18 msec. The small signal loss detected can probably be explained in this way.

In any case, the speed of the switching hardware is certainly fast enough up to phase durations of about 30 msec where we would expect substantial (10%) signal losses to set in. This is more a factor 30 faster than the switching rates employed in other spectroscopic observing modes. It is therefore not obvious whether the data acquisition programs can keep up with this high rate. Experiments made with different backends show that the following minimum phase times apply:

- 1.0 sec for the autocorrelator
- < 20 msec for the 100 kHz filter spectrometer

In the case of the autocorrelator which is equipped with its own processor (a Motorola 68030 running at 25 MHz, a 6882 coprocessor, and 4 Mbyte of onboard memory), the control program in its present form needs about 1 sec to perform the standard calculations, mostly clipping corrections and FFT before data are dumped on the antenna control computer. In the case of the filter spectrometers, data are accumulated in CAMAC latch scalers and read out at the end of each phase by a CAMAC microprocessor and transferred into local memory. This process takes much less than 20 msec for the 100 kHz filter spectrometer.

For FSw observations where only the 100 kHz backend is connected, the maximum switching rate is therefore given by the FSw hardware (~ 30 msec). In the more frequent case where also the correlator is used, the switching rate cannot exceed 1.0 Hz.

4.3 Observing Efficiency

The efficiency of the frequency switching observing mode was measured at two occasions by determining the actual duration of a scan consisting of 10 subscans of 30 seconds each. Fig. 4.1 shows the scan duration for two backend configurations and several phase times. Scan duration is measured as the time elapsed between the moments when the light in the LOAD control button comes on and when the light in the measurement button goes off at the end of the last subscan.

The data obtained with the 100 kHz filters only (open symbols) are found to have very little scatter. For phase times larger than 10 msec, they follow closely the dashed curve. In particular, the scan duration at long phase times is found to be about 350 seconds, giving a FSw observing efficiency of 300/350, or 85% in this mode. At the very shortest phase duration tested, 10 msec, data acquisition fails, because the blanking time is equal to the phase duration. The dashed curve in Fig. 4.1 results from adding to the integration time of the scan (300 sec) overheads due to setup times for the scan and for each of the 10 subscans, and due to a fixed blanking time per phase. After variation of these parameters we obtain the best fit (dashed curve) for the following values: 2 sec of scan overhead, 4 sec subscan overhead, and 10 msec blanking time.

These parameters suggest that most of the combined overhead can be avoided if long subscans are made. Indeed, in an experiment where a 300 sec scan was set up as 2 subscans of 150 sec each (rather than 10 subscans of 30 sec), a total overhead of less than 20 sec was measured, increasing the observing efficiency to $> 90\%$.

The data obtained when the autocorrelator (phase durations > 1 sec only, see section 4.2) was connected in addition to the 100 kHz filters are virtually all above the curve and display a remarkably large scatter. The cause of this additional and variable delay due to the correlator could unfortunately not be investigated.

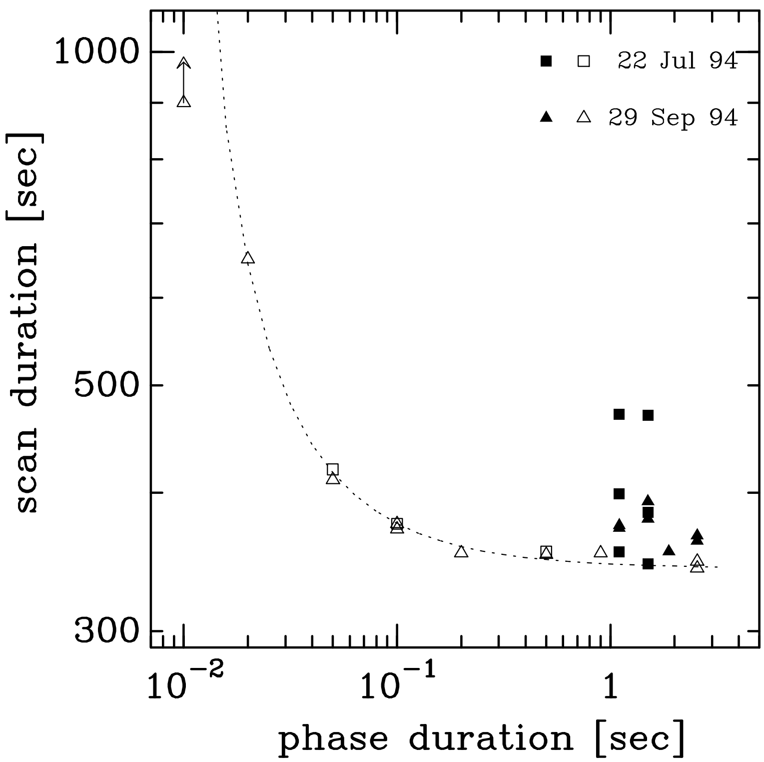

Figure 4.1: Total duration of a scan with 10 subscans of 30 sec integration time. Triangular and square symbols refer to the two independent measurements. In some measurements (open symbols) only the 100 kHz filter spectrometer (parallel mode) was connected, in the other data (filled symbols) both the 100 kHz filters and the autocorrelator (100% of its capacity) were used. The dashed line is the sum of *(i)* the integration time (300 sec), *(ii)* an overhead of 2 sec per scan, *(iii)* an overhead of 4 sec per subscan, and *(iv)* a blanking time of 10 msec per phase.

Chapter 5

Atmospheric features and Frequency Tracking

In frequency switched observations emission or absorption from atmospheric features is not automatically cancelled as it is in the angular switching modes. It is therefore vital to recognise these atmospheric features, the most important of which probably is ^{12}CO(2→1) for the 30m telescope (section 5.1). In section 5.2 these sharp and supposedly rather stable lines are used as an external frequency standard. The precision of the observatory's frequency tracking is measured against this standard.

5.1 Mesospheric CO

CO is a well known constituent of the upper atmosphere. It is distributed over a wide range of heights, between 30 and 70 km, somewhat depending on season and geographic latitude. Line strength and shape of the mesospheric CO (see Fig. 5.1 for an example) are not much different from those of a typical galactic dark cloud. Mesospheric CO is therefore a prime candidate for causing confusion.

Tab. 5.1 lists typical line parameters as observed at the 30m telescope at a few occasions. Although no systematic investigation of the line's dependence on elevation or on season was made, we have evidence that the line strength increases roughly like zenith distance. We do not have data bearing on seasonal dependance, but it has been suggested elsewhere that the mesospheric CO concentration is larger in winter.

We note that these mesospheric CO lines have non–gaussian $3\ldots4$ km s^{-1} line wings at the 10% level. They are easy to detect on the stronger $2 \rightarrow 1$ transition (Fig. 5.1). Our

Table 5.1: Parameters of mesospheric CO as observed at the 30m Telescope

transition	T_A^* [K]	FWHP [km s^{-1}]	elevation [deg.]	date
^{12}CO(1→0)	0.43	0.7	90	30 July 1994
^{13}CO(1→0)	< 0.05		45	29 July 1994
^{12}CO(2→1)	1.9	0.6	90	30 July 1994
^{13}CO(2→1)	< 0.18		45	29 July 1994

measurements furthermore show that the 12/13–isotope ratio is larger than 10, compatible with the terrestrial value of 89. FSw observations of the CO isotopes are therefore considerably less troubled by mesospheric emission.

Note that there probably exist many more mesospheric transitions of other minor atmospheric constituents (e.g. ozone) which may eventually confuse FSw observations.

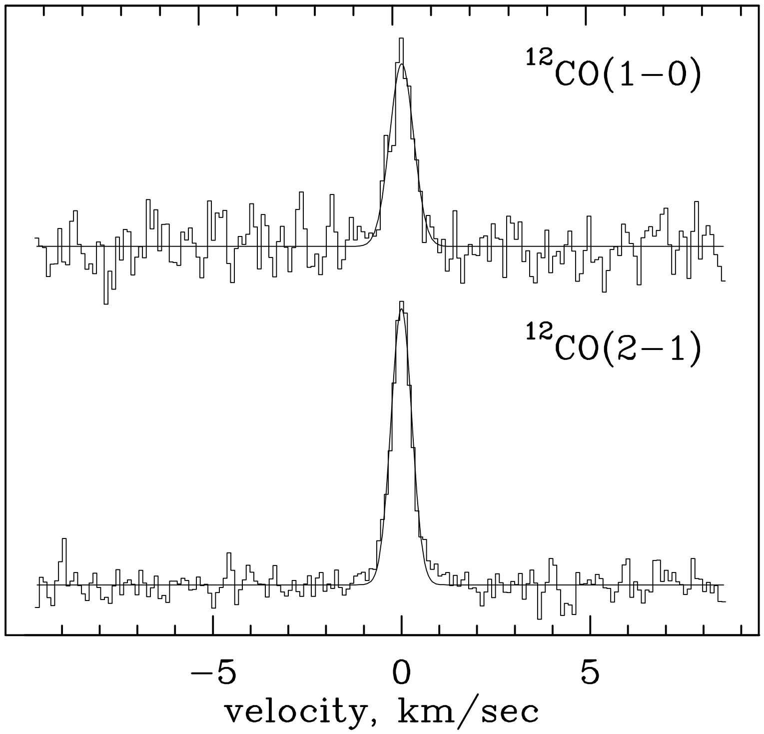

Figure 5.1: Folded FSw spectrum of the 3 and 1 mm transitions of mesospheric ^{12}CO. The observations were made with the 30m telescope parked in zenith position on 30 July 1994 at 4 h UT. Velocity resolution is 0.10 $\mathrm{km\,s^{-1}}$ for both spectra. Integration time is 23 min.

The radial velocities of atmospheric constituents due to weather patterns or global transport phenomena are small for astronomical standards. These constituents therefore appear very closely at rest with respect to the observatory. It is thus an important diagnostic tool to know the observatory's rest velocity in the astronomical frame of reference, often the Local Standard of Rest, LSR. The radial velocity of an atmospheric feature in a particular observation can therefore be obtained by reversing the Doppler correction applied by the antenna control program. The program ASTRO[1] can be used to calculate in advance this Doppler correction for any desired observing direction and date. Below we list a typical such session with ASTRO showing the commands to be typed in after the `ASTRO>` prompt, and the lines printed by ASTRO. The quantity `Dop` gives the instantaneous velocity of the observatory with respect to the sun, projected onto the line of sight to the source (here LkHα101, a star located near the galactic plane at $l = 160°$). The other relevant quantity, `Lsr`, is the projection of the standard solar motion onto the line of sight to the source. The sum of the two quantities, `Dop + Lsr`, is the Doppler correction applied to the rest frequency. The LSR velocity of a mesospheric line will then appear at `-(Dop + Lsr)`. Fig. 5.2 shows this velocity for a few characteristic positions along the galactic plane.

The velocity offsets applied to the rest frequency for a particular subscan by the drive program are also written in the data associated parameter field of the raw data files.

[1]written by R. Lucas and normally included in the package of GAG software.

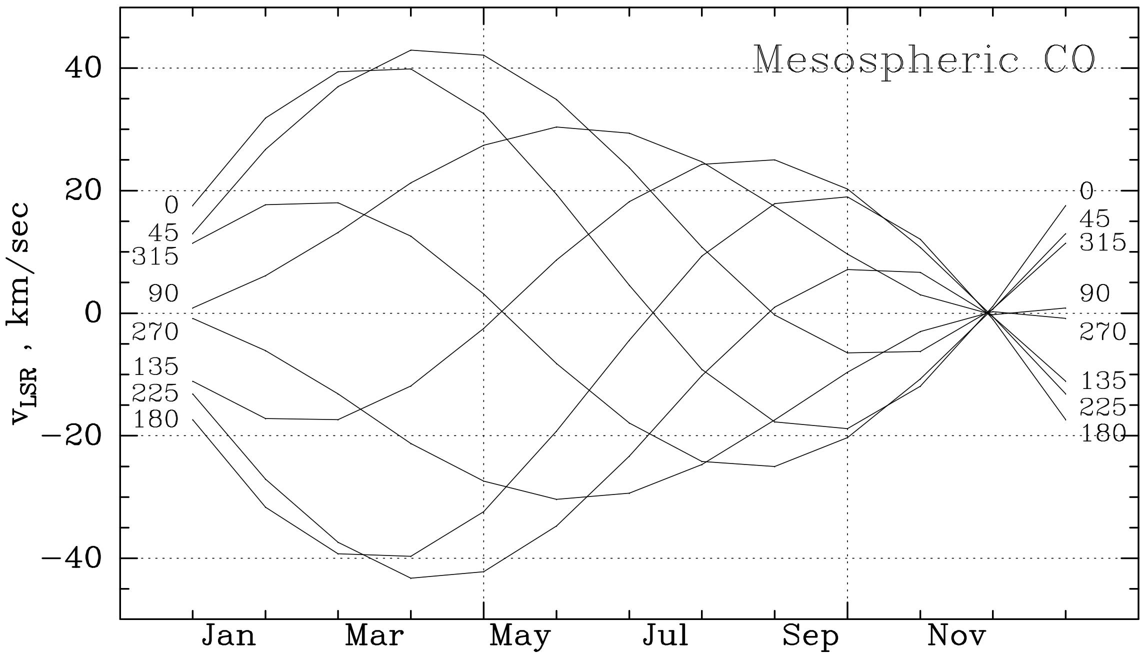

Figure 5.2: Velocity of mesospheric features in the LSR frame. The curves represent observing directions in the galactic plane at the longitude indicated. The ASTRO procedure listed in this section can be used to calculate the velocity in any other direction.

```
Astro> OBSERVATORY veleta
Astro> CATALOG lkha.cat /Veleta
Astro> TYPE  lkha.sou

   LkHa101     eq 1950.0    04:26:27.2      35:09:55      Lsr -2.0

Astro> TIME 13:44:10.0 28-jul-1994/z 2
Astro> HORIZON /SOUR

%  I-OBSERVATORY, Time needs to be reset
   LKHA101: no Sun avoidance period
   LKHA101      Az 103.45725   El 49.12343   Dop = -22.965  Lsr =   7.189
```

5.2 Precision of Frequency Tracking

Since the atmospheric features appear nearly at rest with respect to the Observatory, they can be used as an external frequency standard. In this test, the telescope was parked in the zenith position and the drive program was commanded to Doppler–track a particular quasar during 7 hours around transit. The mesospheric feature, here the strong ^{12}CO(2→1) line, should then appear at the negative velocity offset of the source. The overall precision of the Observatory's frequency tracking — starting from the astronomical ephemeris to the acquisition program, the LO hardware, and including the data reduction program — can then be measured to the accuracy with which the center velocity of the mesospheric ^{12}CO(2→1) can be determined (±10 m/s). Any *vertical* motions of the atmosphere are believed to be smaller than this.

The data obtained are shown in Fig. 5.3. The beginning and end of an integration are connected by a straight line. The observed and commanded velocities never deviate by

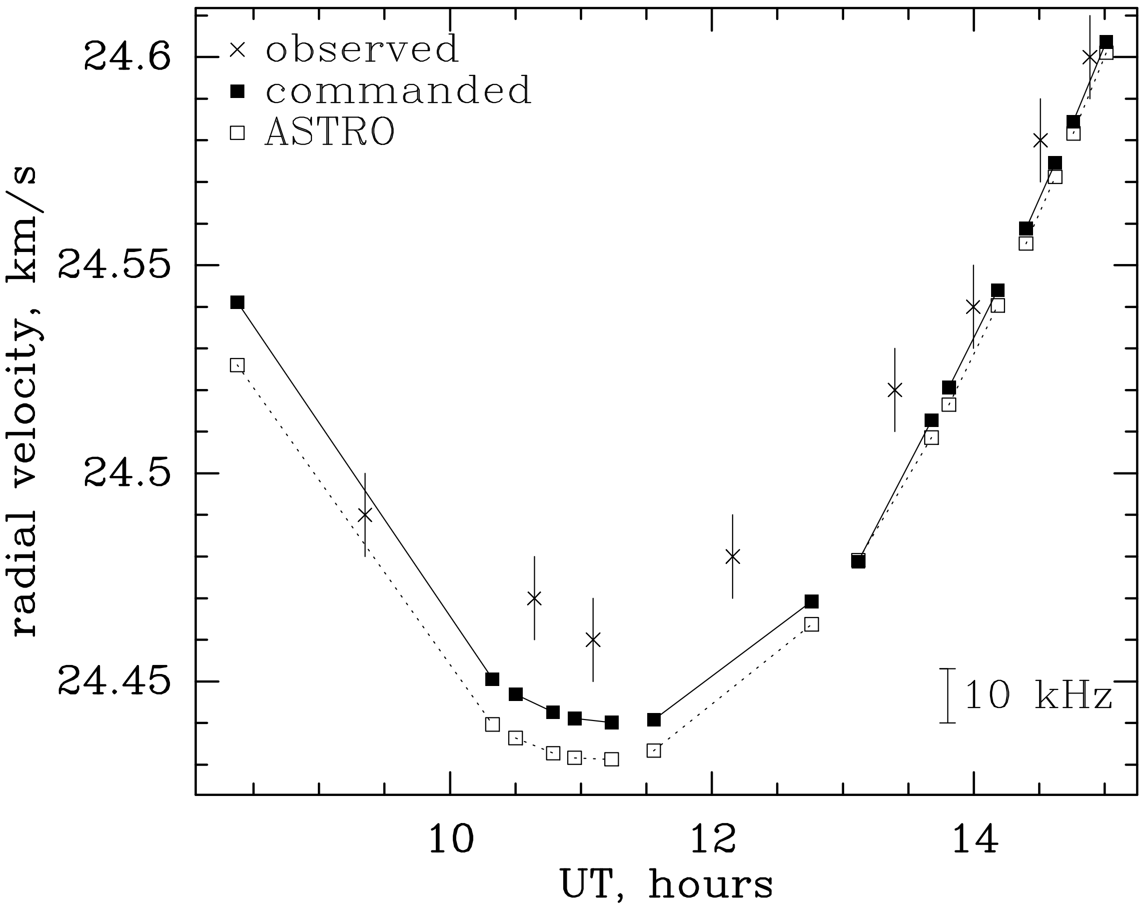

Figure 5.3: Comparison between the Doppler corrections commanded by the 30m drive program, those calculated by the ASTRO software, and those observed from mesospheric $^{12}CO(2\rightarrow1)$ during one day (20 July 1994). During the observations the telescope was parked in zenith position. The drive program Doppler–tracked the quasar 3C273.

more than 2σ, and we conclude that the Doppler tracking is good to 20 m/s ($7 \cdot 10^{-8}$) or better. In terms of frequency, this corresponds to a setting accuracy of better than 15 kHz in the 1mm window. The small, but systematic departure of the observed from the commanded velocities seems to be symmetrical around local noon. Since the precision obtained is thought to be fully sufficient for virtually all FSw observations at the telescope, no further investigations were made of this small discrepancy.

A difference of similar magnitude exists between the velocity corrections calculated by the drive program and those calculated by ASTRO. Some of this difference is actificially introduced, since the drive program calculates the Doppler correction at the beginning of each subscan, whereas the Doppler corrections obtained from ASTRO refer to the time written in the CLASS scan header which refers to the end of a scan. Nevertheless, there seems to exist a small (< 0.01 km s^{-1}) difference between the two programs which might well be due to slight differences in the ephemeris used. These effects, though small enough to be of very little practical importance, need further investigation.

Chapter 6

Conclusions

6.1 Current limitations

Existing hardware and software permit to frequency switch correctly any of the 30m telescope's standard spectral line receivers: `3MM`, `G1`, `2MM`, and `G2`. The `3MM` and `G1` receivers which are served by the main polarization grid in transmission can even be used simultaneously for FSW observations. All the hardware necessary to frequency switch the four spectral line receivers simultaneously and independently is in place. Simultaneous frequency switching with more than two receivers is not yet possible, since the `FSwitch` command of OBS cannot currently handle more than two receivers. Reducing flexibility further, the frontend control program currently requires that the 3mm receiver is always connected, and observations with the `2MM` or the `G2` receiver as a second receiver invoke a manual change of IF cables.

The maximum usable frequency throw is about 45 $\mathrm{km\,s^{-1}}$ on the sky for all receivers, the current exact values are listed in Tab. 4.1.

The range of usable switching rates is normally limited at the slow end to a phase duration of 2.5 seconds. The minimum phase time depends on the kind of backend connected. It is 1.0 seconds for the autocorrelator and of the order of 30 msec for the 100 kHz filter bank. The use of the 1 MHz filterbanks is not recommended for FSw observations.

In all cases investigated, an acceptable quality of the spectroscopic baseline was obtained, provided some precautions were taken. These consist *(i)* in using a frequency throw of 7.7 MHz, the frequency of the dominant baseline ripple, and *(ii)* in setting the Nasmyth optics to a non–standard configuration (Xoptics). Best spectroscopic baselines, comparable in quality to wobbler–switched observations, were obtained when only one receiver was connected, notably the `3MM` receiver owing to its excellent gain stability.

6.2 When to frequency–switch

Despite the various limitations summarized in the preceeding section, there is a wide range of situations when FSw can be, and maybe should be used. Fig. 6.1 gives an example of an efficient FSw observation where three transitions of CO isotopes are observed simultaneously. In this wideband observation (^{13}CO(1→0) and ^{18}CO(1→0) are separated by 419 MHz) the quality of the baseline is, however, somewhat less than average for the C^{18}O(1→0) transition.

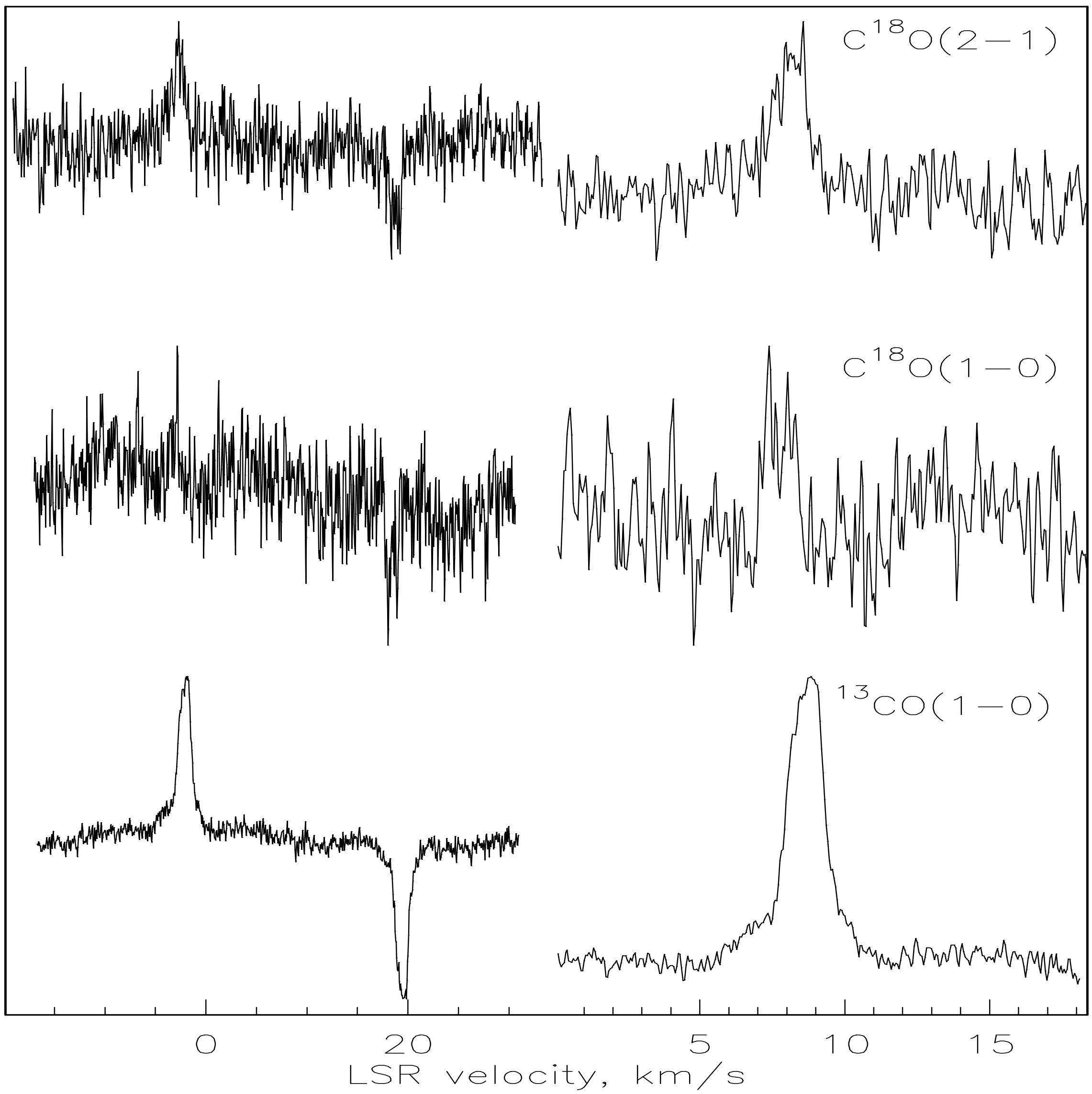

Figure 6.1: Simultaneous observation of 3 lines from a well known source in a nearby star formation region. The left column shows the FSw spectra, the folded spectra are at right. No baselines are removed. Integration time is 120 sec.

In the following, we give a brief checklist of requirements which a planned observation has to fulfill if FSw is to be considered.

- Only the `3MM` and/or the `G1` receivers are presently available for FSw
- trade off between doing PSw or WSw with 3 receivers at low efficiency and FSw with up to 2 receivers at high efficiency
- is the line to be observed narrow enough? As a rule of thumb, the velocity interval over which the emission extends should not be larger than 1/4 of the spectrometer bandwidth or 1/2 of the frequency throw.
- is there any broadband background emission (e.g. galactic plane) ?
- is there confusion with atmospheric emission on the date of the observations?
- are excellent baselines at 1mm essential? This may rule out FSw for particular cases.

6.3 Desirable developments

A central feature of spectroscopic observations with the 30m telescope is that up to 3 (and possibly 4 in the future) receivers can be used in parallel. Our investigation has so far not turned up any fundamental reason why this set of simultaneously observing receivers cannot also be used in a frequency switching mode. For this to work in practice, work has started to extend the corresponding OBS command to handle more than two receivers.

The spectroscopic baseline, although good enough already for many FSw observations, may not be adequate if other than the present two receivers are used for FSw, or if larger throws are used. It appears, however, to be easy to improve on our analysis of the baseline ripple. Observations with spectrometer bandwidths much larger than those used here will unambiguously identify the scattering surfaces, and attempts can then be made to reduce their reflection coefficient.

Observations of positions in the galactic plane where emission can easily extend over more than 30 $\mathrm{km\,s^{-1}}$ are severely confused and not meaningful at all with the current maximum throw. Since such observations are also difficult with the other (angular) switching schemes, it would be very useful to increase the throw of FSw observations. A 50% increase of the current maximum appears possible by using the tuning range of the ADRET synthesizers more efficiently. The limiting element will then most likely be the phase lock units, like it is the case at 3mm now. Ways to improve the performance of this unit should be investigated.

The single most important consideration for a flat spectroscopic baseline is the gain stability of the receiver. The current `3MM` receiver sets a very useful standard. The performance of the other receivers at the 30m is inferior in this respect by a factor of about 3. Stabilization of the LO power will most likely be beneficial in this respect. The effects of instabilities can probably also be reduced by switching faster than the current limit (set by the correlator) of 1 sec which is unfortunately very near the cryogenic pump period. This may require an upgrade of the correlator acquisition program and possibly also new processor hardware.

Some new and potentially interesting FSw observing modes may also require phase durations shorter than 1 second. This implies in practice to make the data aquisition of the autocorrelator substantially faster than at present. Some gain (factor 3?) appears possible if a more modern microprocessor is used. Still smaller phase durations ($\leq$ 0.3 sec) may require a special version of AC aquisition program. In such a version, data would be accumulated for several phases before clipping correction and FFT are calculated.

A typical application of frequency switching is the observation of very extended sources. If efficient mapping of such sources is desired, a new observing mode is needed which combines frequency switching with angular scanning. The scanning could either be done with the telescope or, at higher efficiency on sources smaller than $4'$, with the subreflector.

The price to be paid for the increased efficiency of FSw observations (practically twice that of other observing modes) consists in an increased demand for backend resources. About twice the bandwidth is needed for FSw than for the other observing modes. The number of channels of the autocorrelator, the principal backend in this context, is probably sufficient at present, but may soon turn into a bottleneck. When receivers are equipped with 1 GHz bandwidths, more lines will be observable in parallel, thus increasing the demand on backend channels. The same will happen if FSw should turn out to be possible with more than 2 receivers simultaneously, or if FSw can be made working with larger throws.

Acknowledgement:

We would like to thank Matthew Carter, James Lamb, and Jörn Wink for several discussions and for reading the manuscript. Dave Morris and Carsten Kramer have helped with the analysis of the baseline ripple and other observational aspects. Karl Schuster has donated some of his observing time for testing the three–lines FSw procedure. Wolfgang Wild has stimulated the series of 1994 FSw tests.

Appendix A

OBS procedure file

Below we list the procedure file used with OBS for most of the test observations. The procedure connects two receivers, namely the `3MM` and `G1`, to the 100 kHz filter spectrometer (in parallel mode) and to the autocorrellator, also in parallel mode. The two correlator units are set so that the unit connected to `G1` has twice the bandwidth of the unit connected to `3MM`. In this way, the two units produce spectra with identical velocity resolution and coverage if lines with a 2:1 frequency ratio are observed (Fig. A.1). The correlator is used at a 100% of its capacity (2 units).

The two frequency switch commands make the two receivers switch with a period of 3 sec, the duration of an individual phase is 1.5 sec. Ten such periods are accumulated in one subscan of 30 seconds duration. In this setup, phase 1 is observed with a frequency offset $+\Delta f/2$ and the data are counted positive (weight = +1 in CLASS), whereas phase 2 has $-\Delta f/2$ and is counted negative (weight = −1 in CLASS). The frequency throw Δf is set to 7.7 MHz, the period of the standard telescope ripple at 3mm, and to twice this value at 1mm. In this way, the velocity separation of the positive and negative lines is identical in the two receivers if lines with a 2:1 frequency ratio were observed (Fig. A.1).

```
!LFSw.obs
!LOAD FSW COMMANDS
!..................................SEPTEMBER 94............. CT .....
1M/DISC
2_1M/DISC
100K PAR /RECE 3MM 230G1
AUTO 1 20 40  0.0 /RECE 3MM
AUTO 2 40 80  0.0 /RECE 230G1
FSW 7.7   S /RECE 3MM/PH 1.5/TIME 30
FSW 7.7*2 S /RECE 230G1
```

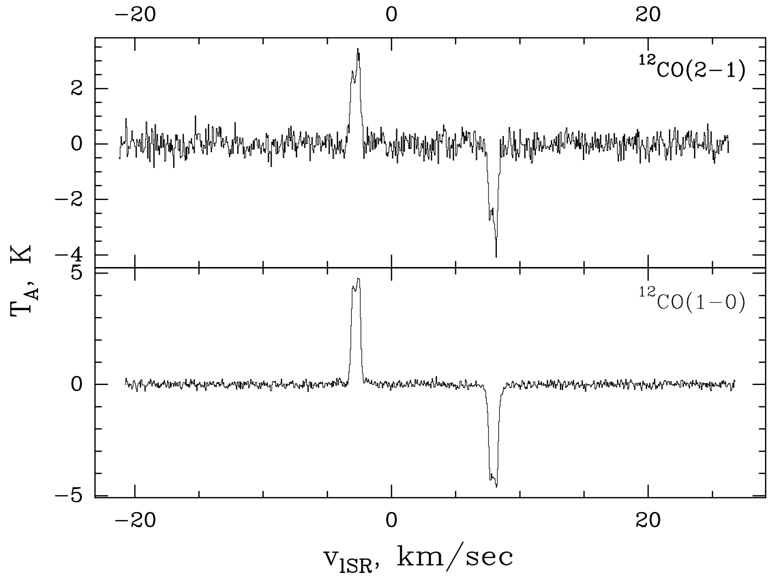

Figure A.1:
Frequency switched observation of CO transition toward the dark cloud L134A with the 1 and 3 mm receivers in parallel. The frequency throw was set to 3.9(7.9) MHz, and the autocorrelator was used with 20 (40) MHz bandwidth and 10(20) kHz resolution for the 1(3)mm transition. Linear baselines were subtracted for clarity. Integration time is 15 min, the 1mm atmospheric opacity was 0.6.

Appendix B

Data reduction

B.1 Calibrated data

The RED process provides an on–line calibration and display of a frequency switched spectrum for each subscan. An average of all such subscans contained in a particular scan is recorded on the OBS/RED output file. This spectrum, i.e. the calibrated difference between phase 1 and phase 2, can then be restored by using the FOLD command of CLASS. This command shifts (in frequency by the `decal[i]` offset) and multiplies (by `poids[i]`) the phase i spectrum, and then adds the spectra of the phases together. Note that the folded spectrum can be contaminated by the 2 spurious signals appearing at inverted temperatures and at half the intensity. The useful baseline range should therefore be restricted to exclude these spurious features.

The relevant frequency switching parameters are recorded in the CLASS header of each scan. They can be looked at and even modified with a procedure like the one listed below.

```
! FSw_variables.class
! CLASS procedure to list the FSw parameters for scan No. &1
!
!..................................... 16-Nov-1994 ...... ct ............
set variable fswitch read
say "scan No." '&1'
say "no. of phases:" 'nphas'

for ii 1 to nphas
    say "phase" 'ii'
    say "  freq. offset, MHz: " 'decal[ii]'
    say "  integr. time, sec: " 'duree[ii]'
    say "  relative weight:   " 'poids[ii]'
next
set variable fswitch off
!.......................................................................
```

B.2 Uncalibrated data

Uncalibrated data are recorded in the observatory's raw data format. These data can be used if an observer wants to calibrate data independently from OBS/RED. The CAL program handles this task. Below we list first a procedure to enter the relevant calibration parameters in CAL, and then a second procedure which calibrates and averages the subscans in one scan.

Contrary to the data file generated by OBS the raw data retains individual subscans and, in each subscan, the data for the individual phases.

```
!calsupply.pro
!procedure to enter calibration parameters in CAL
!
!...................................... 10 Jul 1994 ..... ct ........
 dir  mrt$data:[c01]
 cal auto
 ambient 277 709
 efficiency 0.9 0.9 /rec 3mm
 efficiency 0.9 0.9 /rec 230g1
 chopper 290 77/rec 3mm
 chopper 290 77/rec 230g1
 supply gain_image 0.005 /rec 3mm
 supply gain_image 0.1   /rec 230g1
 supply line 12co(1-0) /rec 3mm
 supply line 12co(2-1) /rec 230g1
!..................................................................
```

```
!cal.pro
!CAL procedure for reducing a FSw scan
!    &1 calibration scan number
!    &2 FSw scan number
!    &3 number of subscans in FSw scan
!
!............................................ 10 Jul 1994 ... ct ......
 cal &1 cold
 scan &2
 c\compute 4 2 !backend 4 (AC), part 2
 for i 1 to &3
   subs i /sig 1 -1 !phase 1 has positive weight, phase 2 negative
   say "subs" 'i'
 next
 plot
!..................................................................
```